PERGAMON

Journal of Geodynamics 33 (2002) 117–129

JOURNAL OF
GEODYNAMICS

www.elsevier.com/locate/jgeodyn

3D reduction of satellite magnetic measurements to obtain magnetic anomaly coverage over Europe

K.I. Kis[a,*], G. Wittmann[b]

[a]*Geophysics Department, Loránd Eötvös University, 1117 Budapest, Pázmány Péter sétány 1/c, Hungary*
[b]*MOL Hungarian Oil and Gas Co. International Exploration and Production, 1117 Budapest Október huszonharmadika u. 18., Hungary*

Abstract

Vector and scalar magnetic anomaly maps have been determined from Magsat data on a spherical grid (35–60° in latitude and −10–30° in longitude) at an altitude of 400 km over the European region. These anomaly maps have been derived using Gaussian and Laplacian weight functions to interpolate the vector and scalar anomaly data. The parameter value of the Gaussian and Laplacian weight functions controls the cut-off wavelength (the shortest wavelength) processed by the interpolation procedures. This parameter value has been determined from the power spectrum of the vector and scalar anomalies of 12 pass sections, covering the European region. The shortest wavelengths for the derivation of the vector and scalar magnetic anomalies have been set at 1000 and 2000 km, respectively. The derived ΔX, ΔY, ΔZ and ΔT maps reflect the regional magnetic anomalies of the European region at the altitude of the Magsat.

1. Introduction

The US Magsat satellite measured vector and scalar magnetic fields of the Earth following a sun-synchronous orbit with inclination 96.76° during the period from 30 October 1979 to 11 June 1980 (Langel et al., 1982a). The results obtained during the last 20 years, the applied data processing, and future perspectives of the satellite magnetic measurements are summarized by Langel and Hinze (1998). One of the aims of the Magsat mission was the derivation of magnetic anomaly maps which reflect the magnetic field of crustal origin. Extensive research has been made for the

* Corresponding author. Tel./fax: +36-1-210-1089.
E-mail address: kisk@ludens.elte.hu (K.I. Kis).

0264-3707/02/$ - see front matter
PII: S0264-3707(01)00058-8

derivation of these kinds of magnetic anomaly maps and their interpretation (e.g. Frey, 1982; Langel et al., 1982b,c; Arkani-Hamed et al., 1994; Ravat et al., 1995).

This paper discusses the derivation of vector and scalar magnetic anomaly maps for the European region. It contributes to a series of papers, presenting the scalar and vector magnetic anomaly maps of Europe (e.g. Meyer et al., 1983; Arkani-Hamed and Strangway, 1986; Nolte and Hahn, 1992; Ravat et al., 1993; Taylor and Ravat, 1995; Kis and Wittmann, 1998).

The Magsat data used for the determination of magnetic anomaly maps were filed on Investigator-B magnetic tapes, obtained from the World Data Center A (control number RG 8800). The applied data processing i.e. the corrections and the data selection is the same as published by Kis and Wittmann (1998). The corrected and selected dawn Magsat data set is used for further computations. The spatial distribution of used data is presented in the authors' above mentioned paper.

An interpolation procedure forms the basic element for the determination of the scalar and vector anomaly maps. In the next section the applied equations of the interpolation procedure will be introduced. Determination of the parameters of the interpolation procedures is based on the spectral analysis of the satellite anomaly data measured along the individual passes of the satellite. Finally, the implementation of the interpolation procedures and the derived magnetic anomaly maps will be presented.

2. Interpolation on a spherical grid

Determination of magnetic anomalies from satellite measurements is considered as a problem of interpolation on a spherical grid. The objective of this section is to outline the procedure of the interpolation methods which can be regarded as 3D filtering of the data.

The satellite data measurements are distributed over a three-dimensional spherical shell. The vector ΔX, ΔY, ΔZ and scalar ΔT anomaly values are obtained by the substruction of the calculated model field values determined from the spherical harmonic model, respectively. This field model (MGS 481 No. 2) was given in the Investigator-B tape for values up to degree and order 14. During this phase of the data processing the magnetic field originating from the Earth's core is removed. In this way the longest wavelength of the anomaly data is also determined, which is approximately 3000 km (Bullard, 1967).

The interpolation equations are presented for the vector ΔX, ΔY, ΔZ and scalar ΔT anomaly values in a spherical coordinate system, respectively. The equations are as follows:

$$\Delta X^{\text{interpolated}}(r, \theta, \lambda) = \sum_{i=1}^{N} w_i \Delta X^{\text{measured}}(r_i, \theta_i, \lambda_i), \tag{1}$$

$$\Delta Y^{\text{interpolated}}(r, \theta, \lambda) = \sum_{i=1}^{N} w_i \Delta Y^{\text{measured}}(r_i, \theta_i, \lambda_i), \tag{2}$$

$$\Delta Z^{\text{interpolated}}(r, \theta, \lambda) = \sum_{i=1}^{N} w_i \Delta Z^{\text{measured}}(r_i, \theta_i, \lambda_i), \tag{3}$$

$$\Delta T^{\text{interpolated}}(r, \theta, \lambda) = \sum_{i=1}^{N} w_i \Delta T^{\text{measured}}(r_i, \theta_i, \lambda_i), \tag{4}$$

where r, θ, λ are the spherical coordinates (radius, colatitude, longitude) of the point of interpolation; w_i, is the weight of the interpolation for the i-th data; and r_i, θ_i, λ_i are the spherical coordinates of the measured point. N is the number of the data used for the interpolation.

Data are interpolated for the spherical grid, ranging from 35 to 60° in latitude, and −10–30° in longitude. The increment in latitude and longitude is 0.2°. The grid is distributed over a sphere with a radius of 6771 km, covering the European region (Fig. 1).

The solution to the interpolation problem includes the determination of the appropriate weight function, and its digitized value, w_i. The interpolation procedure is designed in a three-dimensional spatial frequency domain, and it is implemented in a space domain. The weight function of the interpolation is selected according to the following requirements:

(a) the weight function should be a three-dimensional energy signal, i.e.

$$\int_{-\infty}^{+\infty}\int_{-\infty}^{+\infty}\int_{-\infty}^{+\infty} \left|w(x, y, z)\right|^2 \mathrm{d}x\mathrm{d}y\mathrm{d}z < \infty, \tag{5}$$

and its Fourier transform exists (Bracewell, 1978);

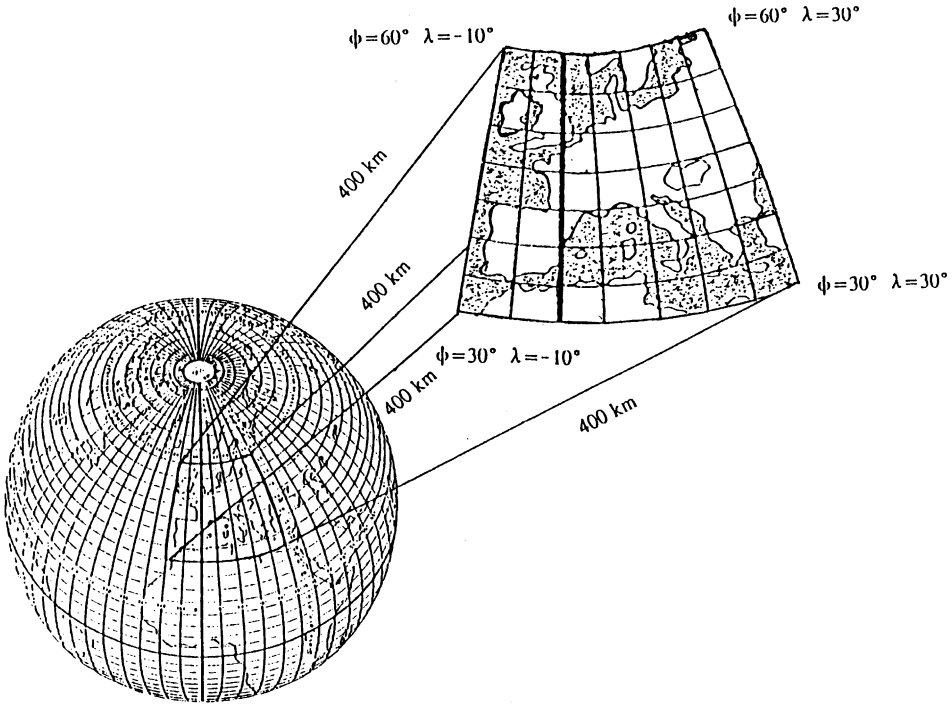

Fig. 1. Schematic view of the spherical surface which is divided into a spherical grid.

(b) the weight function should be spherically symmetrical, which is a non-directive transfer property;
(c) the low-pass property and its cut-off spatial frequency can be defined.

The Gaussian and Laplacian low-pass filters are subject to the requirements (a), (b), and (c) written above. The Gaussian low-pass filter has the additional advantage that the product of signal-duration and frequency-bandwidth is minimum (Bracewell, 1978).

The interpolation is calculated in a three-dimensional Cartesian coordinate system with the x-axis and y-axis oriented North and East, respectively, while the z-axis points vertically downward. The origin of the coordinate system is located at the point at which the value is interpolated. The f_x, f_y, and f_z spatial frequencies are directed in the x-, y-, and z-axis, respectively.

3. Gaussian and Laplacian low-pass filters

The transfer function of the three-dimensional Gaussian low-pass filter in the spatial frequency domain is

$$S^{\text{Gaussian}}_{\text{Low-pass}}(f_r, k) = \exp\left(-(kf_r)^2\right), \tag{6}$$

where f_r is the radial spatial frequency which can be expressed as $f_r^2 = f_x^2 + f_y^2 + f_z^2$. The parameter k controls the cut-off frequency of the Gaussian filter.

The cut-off spatial frequency $f_r^{\text{cut-off}}$ or cut-off wavelength $\lambda^{\text{cut-off}}$ of the interpolation can be defined by the -3 dB attenuation. The relationship between the cut-off spatial radial frequency or cut-off wavelength and the parameter k is given by

$$\text{for} -3\text{dB attenuation } f_r^{\text{cut-off}} = \frac{0.5887}{k} \text{ or } \lambda^{\text{cut-off}} = \frac{k}{0.5887}. \tag{7}$$

The weight function of the Gaussian low-pass filter is obtained from the three-dimensional inverse Fourier transform of the transfer function (6) (Meskó, 1984):

$$w^{\text{Gaussian}}_{\text{Low-pass}}(r, k) = \pi^{3/2}/k^3 \exp\left(-\left(\frac{\pi r}{k}\right)^2\right), \tag{8}$$

where r is the distance between the point of the spherical grid and the data observed.

The transfer function of the three-dimensional Laplacian low-pass filter in the spatial frequency domain is given by

$$S^{\text{Laplacian}}_{\text{Low-pass}}(f_r, \mu) = \exp\left(-\mu|f_r|\right), \tag{9}$$

where the parameter μ controls the cut-off spatial radial frequency. The cut-off spatial frequency or the cut-off wavelength will again be defined by the -3 dB attenuation. The relationship between the cut-off spatial frequency or cut-off wavelength and the parameter μ is given by

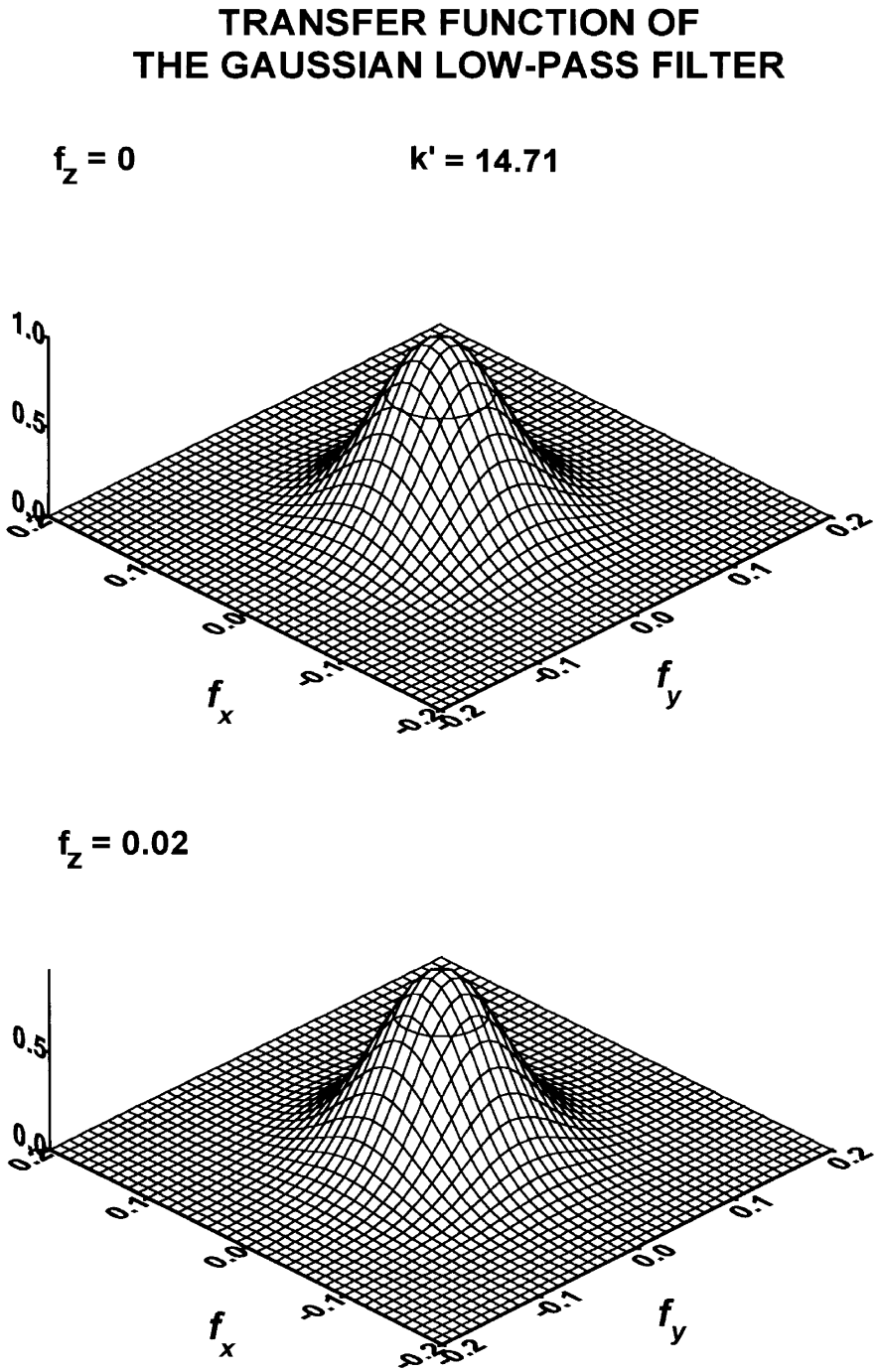

Fig. 2. Surface plot of the transfer function of the Gaussian low-pass filter (the value of the parameter k' is 14.71) versus the dimensionless spatial frequencies f'_x and f'_y, and spatial frequency f'_z fixed at 0, and 0.02, respectively. Horizontal contour shows the -3 dB attenuation.

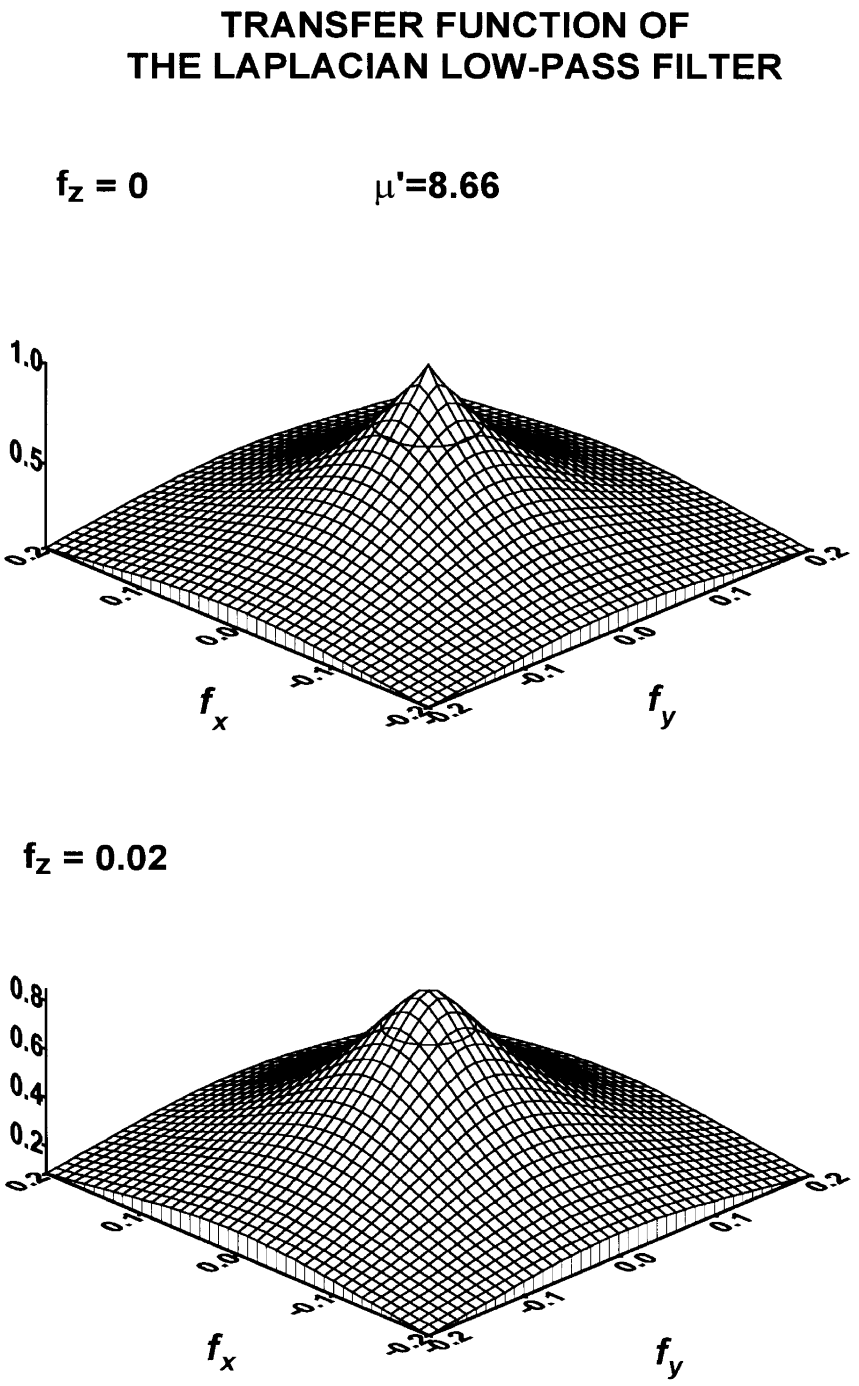

Fig. 3. Surface plot of the transfer function of the Laplacian low-pass filter (the value of the parameter μ' is 8.66) versus the dimensionless spatial frequencies f'_x, and f'_y, and spatial frequency f'_z fixed at 0, and 0.02, respectively. Horizontal contour shows the −3 dB attenuation.

$$\text{for} -3\text{dB attenuation } f_r^{\text{cut-off}} = \frac{0.3466}{\mu} \text{ or } \lambda^{\text{cut-off}} = \frac{\mu}{0.3466}. \tag{10}$$

The weight function of the Laplacian low-pass filter can be obtained now from the three-dimensional inverse Fourier transform of the transfer function (9) (Meskó, 1984):

$$w^{\text{Laplacian}}_{\text{Low-pass}}(r, \mu) = \frac{8\pi\mu}{(\mu^2 + 4\pi^2 r^2)^2}. \tag{11}$$

For numerical calculations, the dimensionless spatial frequency f'_r and the dimensionless parameters k' and μ'; and the dimensionless variable r' are introduced as $f'_r = f_r\xi$, $k' = k/\xi$, $\mu' = \mu/\xi$, and $r' = r/\xi$, where ξ is the sampling interval. The average distance of the measurements over the spherical shell for the dawn data is approximately 40 km (see Kis and Wittmann, 1998).

The transfer function of the Gaussian low-pass filter is displayed on a surface plot versus the dimensionless spatial frequencies f'_x and f'_y for $f'_z = 0$, and $f'_z = 0.02$, respectively (Fig. 2). For a cut-off wavelength of 1000 km, the value of the parameter k' is 14.71 [Eq. (7)]. Determination of the parameter k' will be given in the next section. The solid horizontal contour in Fig. 2 indicates the value of the -3 dB attenuation of the transfer.

The transfer function of the Laplacian low-pass is displayed on a surface plot versus the dimensionless spatial frequencies f'_x and f'_y for $f'_z = 0$, and $f'_z = 0.02$, respectively (Fig. 3). When the value of the parameter μ' is set to 8.66, it means that the cut-off wavelength of the interpolation is 1000 km. Determination of the parameter μ' will be given in the next section. The solid horizontal contour in Fig. 3 indicates the value of the -3 dB attenuation of the transfer.

Table 1
Position of six dawn pass sections (19,433,588,911,1437,1438) and six dusk pass sections (1072,1397,1430,1460,1849, 2096)

Pass number	Starting coordinates of the pass section			Ending coordinates of the pass section			Number of the data
	Latitude	Longitude	Radius	Latitude	Longitude	Radius	
19	60.90°	14.75°	6726.61 km	13.72°	0.94°	6763.56 km	149
433	67.14°	42.60°	6809.32 km	12.15°	23.97°	6900.17 km	176
588	67.02°	19.20°	6861.38 km	12.60°	0.73°	6911.39 km	176
911	69.75°	45.28°	6881.45 km	14.98°	24.59°	6830.18 km	172
1072	23.75°	57.92°	6876.79 km	73.32°	34.13°	6871.77 km	165
1397	21.98°	58.39°	6845.68 km	75.79°	29.50°	6764.86 km	176
1430	21.86°	11.57°	6835.60 km	76.68°	−19.56°	6751.98 km	163
1437	61.36°	38.13°	6713.47 km	13.55°	24.12°	6719.95 km	149
1438	62.12°	14.76°	6713.23 km	13.31°	0.85°	6720.21 km	149
1460	22.02°	34.55°	6825.55 km	77.24°	1.89°	6741.70 km	177
1849	24.89°	10.69°	6708.64 km	65.55°	−3.93°	6702.07 km	127
2096	26.60°	57.25°	6715.14 km	73.43°	34.03°	6756.63 km	149

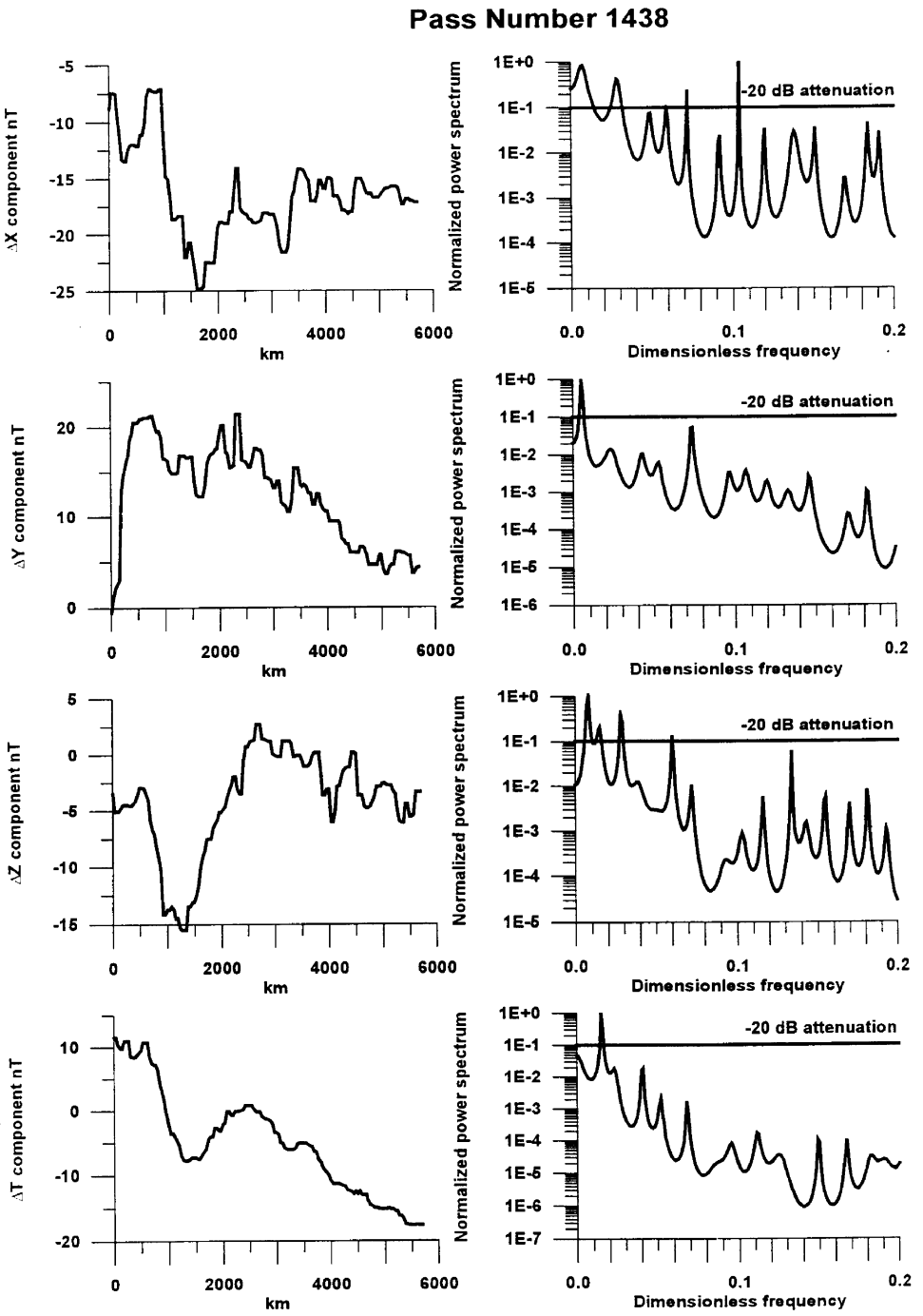

Fig. 4. The ΔX, ΔY, ΔZ and ΔT anomaly data of the pass section 1438, plotted as a function of distance from the starting point. The normalised power spectra of the corresponding anomalies are plotted as a function of the dimensionless spatial frequency on a logarithmic scale. The -20 dB attenuation of the power spectra is indicated in the plots.

4. Spectral analysis of the Magsat anomalies

The determination of the parameters k and μ of the interpolation functions requires some considerations. The spectral analysis of the anomaly values yields the basis of the certain considerations.

Data have been obtained at equidistant intervals of 40 km (approximately) along the passes. The number of the discrete Magsat data points along each pass for the European area varies between 100 and 200. Assuming the measured data along the European section of passes as an autoregressive process, enables the power spectrum of such a processes to be determined by means of the technique of maximum entropy spectral analysis (Ulrych and Bishop, 1975; Ulrych and Clayton, 1976). This method has produced considerable success on the analysis of different geophysical time series (e.g. Currie, 1973; Courtillot and Le Mouël, 1976; Jin and Thomas, 1977, etc.).

There are several effective computer algorithms for the implementation of maximum entropy spectral analysis: the Burg, and the Yule-Walker procedures suggested by Ulrych and Bishop (1975); a different approach is presented by Barrodale and Erickson (1980a,b); an application of Marple's algorithm is suggested by Barrodale et al. (1983). We applied Marple's algorithm to determine the power spectrum of Magsat vector and scalar anomalies, respectively.

The power spectrum of ΔX, ΔY, ΔZ and ΔT for 12 pass sections will now be discussed. The data obtained from 6 dawn, and 6 additional dusk pass sections were spectrum analysed by means of maximum entropy. Table 1 contains the starting and ending coordinates of these pass sections. It is apparent from Table 1 that certain pairs of pass sections are relatively close to each other. Pass numbers of these pass sections are as follows: 19–1438, 433–911 for the dawn data; and 1072–1397, 1460–1849 for the dusk data, respectively. Fig. 4 shows the ΔX, ΔY, ΔZ and ΔT anomalies of the dawn pass section 1438, plotted versus distance measured along the track.

The aim of the spectrum analysis was to determine the upper spatial frequency or shortest wavelength with a power spectrum corresponding to a value of -20 dB attenuation. As an example, for the vector and scalar data of the dawn pass section 1438 the following results have been obtained: the characteristic shortest wavelength is 400 km for the ΔX component; 517 km

Table 2
Shortest wavelength of the anomalies determined by spectral analysis

Pass number	Meridian	Shortest wavelength in				K_p index
		ΔX Anomalies	ΔY Anomalies	ΔZ Anomalies	ΔT Anomalies	
19	Dawn	570 km	1300 km	1200 km	1600 km	1_0
433	Dawn	1300 km	800 km	1060 km	1600 km	2_-
588	Dawn	690 km	670 km	1600 km	1330 km	1_+
911	Dawn	800 km	900 km	1200 km	2600 km	2_+
1072	Dusk	1140 km	890 km	800 km	4000 km	1_+
1397	Dusk	1380 km	640 km	1170 km	4000 km	1_+
1430	Dusk	800 km	570 km	1290 km	1200 km	1_+
1437	Dawn	730 km	1600 km	570 km	1330 km	1_0
1438	Dawn	400 km	517 km	660 km	1900 km	1_0
1460	Dusk	1820 km	400 km	300 km	1140 km	0_+
1849	Dusk	670 km	1000 km	800 km	2660 km	2_0
2096	Dusk	2220 km	1330 km	1050 km	1000 km	1_0

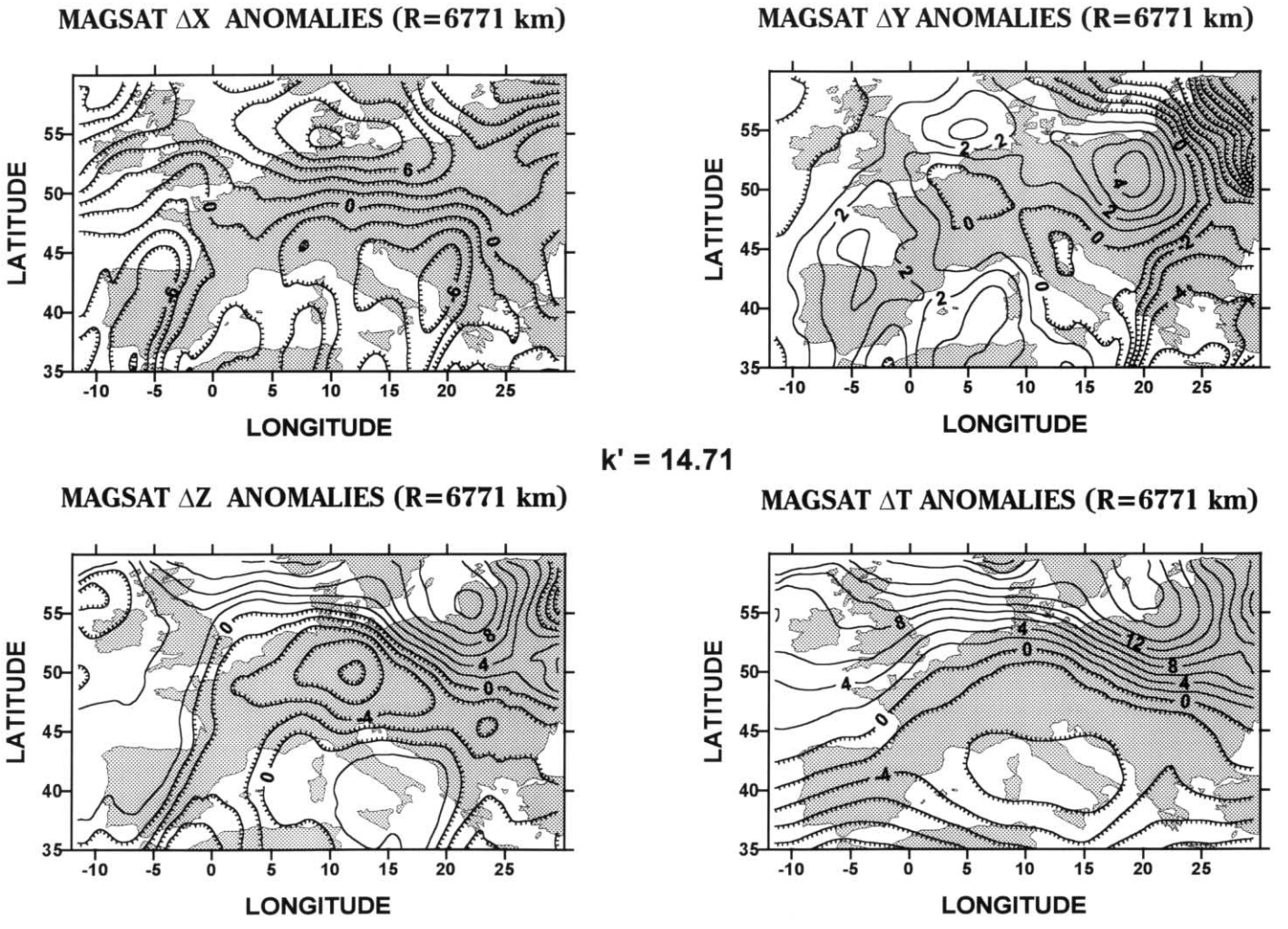

Fig. 5. Contour plots of interpolated vector and scalar anomalies (the Gaussian weight function is applied for the interpolation) for the European region on a sphere with radius of 6771 km. The contour interval is 2 nT, while negative values are indicated by downhill hachures, plotted on an equidistant cylindrical projection.

for the ΔY component; 660 km for the ΔZ component, and 1900 km for the ΔT field, respectively. The normalized power spectrum of the vector and scalar data of this particular pass section is also shown in Fig. 4. The power spectra are plotted versus the dimensionless spatial frequency for the interval of 0–0.2. The position of the dawn pass section numbered 19 is close to the position of the previously discussed pass section of 1438. The spectral analysis of the ΔX, ΔY, ΔZ and ΔT data, however, shows different characteristic upper spatial frequencies. Table 2 contains the shortest wavelength determined from the power spectrum for the data of the pass sections presented in Table 1. From this we can conclude that:

- the noise level for the scalar data is less than that of the vector data, it probably expresses the higher error budget of the vector data (Langel et al., 1982a; Langel and Hinze, 1998);
- the noise levels of the analysed dusk and dawn data do not differ significantly;
- the effect from perturbations as characterised by the K_p index (up to 2_0) is not detectable in the noise level (it should be noted the data used in this analysis are in the latitude interval of 13–69° approximately);
- the low spatial frequency band of the power spectra is dominant in some cases.

5. Magnetic anomaly maps

The vector and scalar magnetic anomaly maps as derived from our interpolation procedure for a spherical grid are presented in this section. The altitude of the spherical grid is 400 km which corresponds to the average altitude of the Magsat satellite. The radius of the three-dimensional sphere (which surrounds a grid point) is determined by the decrease of the weight function for its 0.01 fraction. This requirement determines the number of the data points used for interpolation.

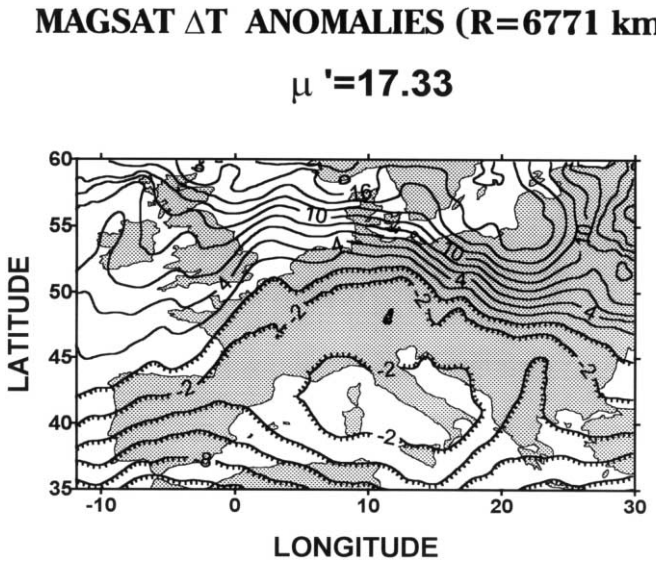

Fig. 6. A contour plot of interpolated scalar anomalies (the Laplacian weight function is applied for the interpolation) for the European region on the surface of a sphere of the radius of 6771 km. The contour interval is 2 nT, while negative values are indicated by downhill hachures, using an equidistant cylindrical projection.

The corresponding values of the parameters k' and μ' were obtained from the power spectrum of the analysed pass sections. A value of 1000 km is considered to be an appropriate shortest wavelength based on the results presented in Table 2 for the both ΔZ and ΔT anomalies. For this shortest wavelength the parameter value for the Gaussian low-pass filter is set to 14.71 [see Eq. (7)]. This Gaussian low-pass filter was then applied as the weight function of the interpolation procedure to derive the ΔX, ΔY, ΔZ and ΔT magnetic anomaly maps shown in Fig. 5. These maps represent the regional character (for the wavelength range between 3000 and 1000 km) of magnetic anomalies over the European region at satellite altitude.

The total magnetic anomaly for the European region, shown in Fig. 6, is derived using the Laplacian weight function interpolation procedure with a cut-off wavelength set at 2000 km. The parameter value μ' is 17.33 accordingly set to [see Eq. (10)]. The regional character (for the wavelength range between 2000 and 3000 km) of the total magnetic anomalies present in the European region, can be clearly seen.

The interpretation of the ΔZ anomalies determined by the suggested method was discussed by the present authors (Kis and Wittmann, 1998). The following characteristic regional magnetic anomalies can be recognized in Figs. 5 and 6. The Tornquist–Teisseyre tectonic line is indicated by a high gradient zone in the northeast part of the ΔZ and ΔT maps. The magnetic low is in the middle part of the European continent. It correlates with the north Germano-Polish depression which is called the Central European Magsat low by Ravat et al. (1993). The magnetic high zone (in the central part of the vertical magnetic anomaly map and a relative high zone in the central part of the total magnetic anomaly maps) is located in the south of Italy. They correspond to the area of low heat flow a thicker lithosphere (Della Vedova et al., 1991)

Acknowledgements

The authors are indebted to Dr. W.B. Agocs and Dr. P.T. Taylor for their encouragement and the detailed discussion of the material. This research was supported by the OTKA (Hungarian Scientific Research Fund) Project No. T 025799. The award of the project is highly acknowledged.

References

Arkani-Hamed, J., Langel, R.A., Purucker, M., 1994. Scalar magnetic anomaly maps of Earth derived from POGO and Magsat data. J. Geophys. Res. 99 (B12), 24075–24090.

Arkani-Hamed, J., Strangway, D.W., 1986. Magnetic susceptibility anomalies of lithosphere beneath eastern Europe and the Middle East. Geophysics 51, 1711–1724.

Barrodale, I., Delves, L.M., Erickson, R.E., Zala, C.A., 1983. Computational experience with Marple's algorithm for autoregressive spectrum analysis. Geophysics 48, 1274–1286.

Barrodale, I., Erickson, R.E., 1980a. Algorithms for least-square linear prediction and maximum entropy spectral analysis—Part I: theory. Geophysics 45, 420–432.

Barrodale, I., Erickson, R.E., 1980b. Algorithms for least-square linear prediction and maximum entropy spectral analysis—Part II: Fortran program. Geophysics 45, 433–446.

Bracewell, R.N., 1978. The Fourier Transform and Its Applications. McGraw-Hill, New York.

Bullard, E.C., 1967. The removal of trend from magnetic surveys. Earth Planet. Sci. Lett. 2, 293–300.

Courtillot, V.E., Le Mouël, J.-L., 1976. Time variations of the Earth's magnetic field with a period longer than two months. Phys. Earth Planet. Inter. 12, 237–240.

Currie, R.G., 1973. Geomagnetic line spectra—2 to 70 years. Astrophys. Space Sci. 21, 425–438.

Della Vedova, B., Marson, I., Panza, G.F., Suhadolc, P., 1991. Upper mantle properties of Tuscan–Tyrrhenian area: a framework for its recent tectonic evolution. Tectonophysics 195, 311–318.

Frey, H., 1982. Magsat scalar anomaly distribution. Geophys. Res. Lett. 9, 277–280.

Jin, R.S., Thomas, D.M., 1977. Spectral line similarity in the geomagnetic dipole field variations and length of day fluctuations. J. Geophys. Res. 82, 828–834.

Kis, K.I., Wittmann, G., 1998. Determination of vertical magnetic anomalies and equivalent layer for the European region from the Magsat measurements. J. Appl. Geophys. 39, 11–24.

Langel, R.A., Hinze, W.J., 1998. The Magnetic Field of the Earth's Lithosphere, the Satellite Perspective. Cambridge University Press, Cambridge.

Langel, R.A., Ousley, G., Berbert, J., Murphy, J., Settle, M., 1982a. The Magsat mission. Geophys. Res. Lett. 9, 243–245.

Langel, R.A., Phillips, J.D., Horner, R.J., 1982b. Initial scalar magnetic anomaly map from Magsat. Geophys. Res. Lett. 9, 269–272.

Langel, R.A., Schnetzler, C.C., Phillips, J.D., Horner, R.J., 1982c. Initial vector magnetic anomaly map from Magsat. Geophys. Res. Lett. 9, 273–276.

Meskó, A., 1984. Digital Filtering Applications in Geophysical Exploration for Oil. Akadémiai Kiadó, Budapest.

Meyer, J., Hufen, J.H., Siebert, M., Hahn, A., 1983. Investigation of the internal geomagnetic field by means of a global model of the Earth's crust. J. Geophys. 52, 71–84.

Nolte, H.J., Hahn, A., 1992. A model of the distribution of crustal magnetization in central Europe compatible with the field of magnetic anomalies deduced from Magsat results. Geophys. J. Int. 111, 483–496.

Ravat, D.N., Hinze, W.J., Taylor, P.T., 1993. European tectonic features observed by Magsat. Tectonophysics 220, 157–173.

Ravat, D.N., Langel, R.A., Purucker, M., Arkani-Hamed, J., Alsdorf, D.E., 1995. Global vector and scalar Magsat magnetic anomaly maps. J. Geophys. Res. 100 (B10), 20111–20136.

Taylor, P.T., Ravat, D.N., 1995. An interpretation of the Magsat anomalies of central Europe. J. Appl. Geophys. 34, 83–91.

Ulrych, T.J., Bishop, T.N., 1975. Maximum entropy spectral analysis and autoregressive decomposition. Rev. Geophys. Space Phys. 13, 183–200.

Ulrych, T.J., Clayton, R.W., 1976. Time series modelling and maximum entropy. Phys. Earth Planet. Inter. 12, 188–200.